A Statistical Analysis of Shape Reconstruction from Areas of Shadows*

Amyn Poonawala,[1] Peyman Milanfar,[2] and Richard. J. Gardner[3]

[1]Computer Engineering Department, University of California, Santa Cruz, CA 95064, amyn@soe.ucsc.edu

[2]Electrical Engineering Department, University of California, Santa Cruz, CA 95064, milanfar@ee.ucsc.edu

[3]Mathematics Department, Western Washington University, Bellingham, WA 98825, Richard.Gardner@wwu.edu

Abstract

We present a statistical analysis of the problem of shape reconstruction from measurements of the brightness function (areas of shadows) by deriving the Cramér-Rao lower bound (CRLB) on the estimated 2-D boundary. Confidence region techniques are used to analyze and visualize the performance of the 2-D parametric shape estimation problem. The brightness function data is very weak, so we have to use a constrained CRLB on the shape parameters to form the confidence regions. Algorithms for reconstructing the shape of a convex object from multiple measurements of its brightness function were developed in [2] and [3]. The Cramér-Rao bound analysis presented here provides statistical estimates that can be used for performance evaluation of these algorithms.

1 Introduction

The problem we consider is that of shape reconstruction from noisy measurements of the brightness function. The brightness function of an n-dimensional body gives the volumes of its $(n-1)$-dimensional orthogonal projections (i.e., shadows) on hyperplanes. The discussion in this paper is restricted to 2-dimensional bodies, in which case the brightness function gives the lengths of the orthogonal projections of the shape on lines. In this context it is natural to work with convex bodies, that is, convex sets with non-empty interiors. The problem is an inverse problem in the area of geometric tomography; see [1, Problem 3.6]. Related problems in tomography that have been studied in the past include reconstruction using Radon transforms, or using support functions (as in [6]). Brightness functions, however, constitute a much weaker form of data. In this paper we provide a statistical analysis of this estimation problem using the Cramér-Rao lower bound.

*Supported in part by U.S. National Science Foundation grants CCR-9984246

2 Background

The brightness function $b(v)$ of a suitably smooth convex body for a given viewing direction v (a unit vector) is given by

$$b(v) = \frac{1}{2}\int |u^T v| f(u) du, \tag{1}$$

where $f(u)$ is the extended Gaussian image (EGI) of the body. Integration is over the unit sphere (in two dimensions, the unit circle). The function f is actually just the reciprocal of the curvature at the point on the boundary where u is the outer unit normal vector. (For more details, see [2], [3], and [4].)

Whether the body is smooth or not, our approach is to reconstruct an approximating polygon that best matches the measured brightness data in the least-squares sense. For a convex polygon with N edges we have the following formula corresponding to (1):

$$b(v) = \frac{1}{2}\sum_{k=1}^{N} a_k |u_k^T v|, \tag{2}$$

where a_k denotes the length of kth edge and u_k denotes the outer unit normal to the kth edge. If $v = [\cos\alpha, \sin\alpha]^T$ and $u_k = [\cos\theta_k, \sin\theta_k]^T$, we can rewrite (2) in the form

$$b(\alpha) = \frac{1}{2}\sum_{k=1}^{N} a_k |\cos(\alpha - \theta_k)|. \tag{3}$$

The problem is to estimate the shape parameters $a_1, \ldots, a_N$ and $\theta_1, \ldots, \theta_N$ (i.e., the EGI of the polygon) using corrupted brightness functions measured from multiple viewing directions. The data obtained is very weak, and there can be infinitely many convex bodies having the same (exact) brightness function measurements in all viewing directions; see [3]. However, Aleksandrov's projection theorem [1, Theorem 3.3.6] says that any two origin-symmetric convex bodies having same brightness functions must be

0-7803-7576-9/02$17.00

equal. Hence we seek to reconstruct origin-symmetric bodies to overcome the non-uniqueness problem.

The corrupted brightness function measurements are modeled by $b(\alpha_m) + n(\alpha_m)$, $m = 1, \ldots, M$, where the first term is given by (3) and the second term is the noise. The problem of finding the parameters $a_1, \ldots, a_N$ and $\theta_1, \ldots, \theta_N$ from the measurements can be solved using constrained non-linear optimization, where the constraints are as follows:

$$a_1, \ldots, a_N \geq 0; \tag{4}$$

$$a_k = a_{N/2+k} \text{ for } k = 1, \ldots, N/2; \tag{5}$$

$$\theta_k = \theta_{N/2+k} + \pi \text{ for } k = 1, \ldots, N/2. \tag{6}$$

Constraints (5) and (6) ensure that the output polygon will be origin symmetric (note that N is even in this case). Details can be found in [3], where a linear optimization approach due to Markus Kiderlen is also described.

3 The Cramér-Rao lower bound

The Cramér-Rao lower bound (CRLB) is a statistical tool often used in the performance evaluation of estimation problems. It provides the theoretical lower bound on the variance of any unbiased estimator; see, for example, [5, pp. 27–35]. Since no unbiased estimator can have lower variance than the CRLB, it provides a benchmark for comparison in the performance of an algorithm.

Consider an observation vector X given by

$$X = f(\psi) + W,$$

where $\psi = [\psi_1, \ldots, \psi_P]^T$ is the vector of parameters to be estimated and W is the noise. The CRLB (see [5, pp. 30–44]) states that the covariance matrix is bounded below as follows:

$$\mathrm{Cov}(\hat{\psi}) \geq J^{-1}(\psi). \tag{7}$$

Here $\hat{\psi}$ is the vector of estimated parameters and $J(\psi)$ is a $P \times P$ matrix called the Fisher information matrix (FIM), whose entries are given by the following expression involving the probability density function (p.d.f.) $p(X; \psi)$ of the observed data:

$$J(i,j) = J(\psi)_{ij} = -E\left(\frac{\partial^2 \ln p(X;\psi)}{\partial\psi_i \partial\psi_j}\right), \tag{8}$$

for $i, j = 1, \ldots, P$.

The noise corrupting the brightness function measurements is assumed to be $N(0, \sigma^2)$. Therefore, the p.d.f. for the brightness function data is

$$p(X;\psi) = \prod_{m=1}^{M} \frac{1}{\sqrt{2\pi\sigma^2}} \exp\left[\frac{-1}{2\sigma^2}\left(b(\alpha_m) - \frac{1}{2}\sum_{k=1}^{N} a_k |\cos(\alpha_m - \theta_k)|\right)^2\right], \tag{9}$$

where $X = [b(\alpha_1), \ldots, b(\alpha_M)]^T$ and $\psi = [a_1, \ldots, a_N, \theta_1, \ldots, \theta_N]^T$ is the parameter vector of length 2N. Therefore the FIM will be a $2N \times 2N$ matrix consisting of four $N \times N$ blocks J_1, J_2, J_3, and J_4. Specifically, for $i, j = 1, \ldots, N$, we have

$$J_1(i,j) = J(i,j) = -E\left(\frac{\partial^2 \ln p(X;\psi)}{\partial a_i \partial a_j}\right), \tag{10}$$

$$J_2(i,j) = J(i,j+N) = -E\left(\frac{\partial^2 \ln p(X;\psi)}{\partial a_i \partial \theta_j}\right), \tag{11}$$

$$J_3(i,j) = J(i+N,j) = -E\left(\frac{\partial^2 \ln p(X;\psi)}{\partial \theta_i \partial a_j}\right), \tag{12}$$

and

$$J_4(i,j) = J(i+N,j+N) = -E\left(\frac{\partial^2 \ln p(X;\psi)}{\partial \theta_i \partial \theta_j}\right). \tag{13}$$

Using (8), (9) and (10)–(13), we find (see [7]) that

$$J_1(i,j) = \frac{1}{4\sigma^2}\sum_{m=1}^{M} |c_{m,i}|\,|c_{m,j}|, \tag{14}$$

$$J_2(i,j) = \frac{a_j}{4\sigma^2}\sum_{m=1}^{M} |c_{m,i}|\, s_{m,j}\,\mathrm{sgn}(c_{m,j}), \tag{15}$$

$$J_3(i,j) = \frac{a_i}{4\sigma^2}\sum_{m=1}^{M} |c_{m,j}|\, s_{m,i}\,\mathrm{sgn}(c_{m,i}), \tag{16}$$

and

$$J_4(i,j) = \frac{a_i a_j}{4\sigma^2}\sum_{m=1}^{M} s_{m,i}\, s_{m,j}\,\mathrm{sgn}(c_{m,i})\,\mathrm{sgn}(c_{m,j}), \tag{17}$$

where $c_{m,k} = \cos(\alpha_m - \theta_k)$, $s_{m,k} = \sin(\alpha_m - \theta_k)$ and $\mathrm{sgn}(f)$ returns +1 or -1 according to whether f takes positive or negative values, respectively. Thus, J is a function of ψ, the vector of shape parameters, and the set of viewing directions used to measure the brightness function.

The lower bound on the variance of the shape parameters for any input polygon can be obtained by computing the FIM from (14)–(17), inverting this matrix, and using the CRLB (7). However, we observed that irrespective of the input polygon, the FIM turns

out to be singular, yielding an infinite lower bound. The reason for this behavior is that the constraints (4)–(6) for the estimation problem have not been taken into account. The infinite CRLB reflects the fact, mentioned above, that the solution is not unique unless these constraints are imposed. In the next section we describe how to deal with this issue.

4 The constrained Cramér-Rao lower bound

The non-uniqueness issue was overcome in [3] by reconstructing an origin-symmetric output body. Similarly, we need to incorporate the constraints (5) and (6) for origin symmetry in the CRLB analysis to get sensible results. We use the method given in [8], a constrained Cramér-Rao lower bound (CCRLB) analysis, which is appropriate for such problems.

Let $g_i(\psi) = 0$, $i = 1, \ldots, K$, where $\psi \in \Re^P$ and $K < P$, be equality constraints defined by continuously differentiable functions, and let $g(\psi) = (g_1(\psi), \ldots, g_K(\psi))^T$ be the corresponding constraint vector. The gradient matrix of g is a $K \times P$ matrix defined by

$$G(\psi) = \frac{\partial g(\psi)}{\partial \psi^T},$$

where G should have full rank. Let $U \in \Re^{P \times (P-K)}$ be an orthogonal matrix in the null space of $G(\psi)$. Then

$$G(\psi)U = 0.$$

The analysis in [8] shows that, under the given constraints, the covariance matrix of the estimated parameters should now satisfy

$$\mathrm{Cov}(\hat{\psi}) \geq U(U^T J U)^{-1} U^T. \tag{18}$$

For an N-sided polygon, we have N equality constraints given by (5) and (6), so the gradient matrix of constraints is an $N \times 2N$ matrix. For example, when $N = 6$, we have

$$G(\psi) = \begin{bmatrix} T_6 & 0 \\ 0 & T_6 \end{bmatrix}$$

where T_6 is the Toeplitz matrix

$$T_6 = \begin{bmatrix} 1 & 0 & 0 & -1 & 0 & 0 \\ 0 & 1 & 0 & 0 & -1 & 0 \\ 0 & 0 & 1 & 0 & 0 & -1 \end{bmatrix}.$$

After carrying out the analysis discussed in this section, we will be able to obtain the CCRLB for the shape parameters. However, our final aim is to reconstruct the 2-D shape using brightness function measurements and not simply to find these parameters. Therefore, after finding the CCRLB, we proceed to find confidence regions of the estimated shape.

5 Confidence regions

Asymptotic global confidence region techniques are used to analyze and visualize the performance of 2-dimensional parametric shape estimators. Assuming a maximum likelihood estimator (MLE) operating in the asymptotic regime, the CRLB for the shape parameters can be used to define a confidence region around the true boundary of the shape, as in [9]. Note that the MLE is asymptotically normal and asymptotically attains the CRLB; see [5, pp. 164–167]. We follow [9] below; in our analysis, however, we have used instead the CCRLB for the shape parameters.

Consider a 2-D shape parametrization of the form

$$s(t;\psi) = [s_x(t;\psi), s_y(t;\psi)]^T,$$

where s is the boundary parametrized by $t \in [0, T]$, and s_x and s_y give the x and y coordinates. Here $\psi \in \Re^P$ is the P-dimensional parameter vector. At each point along the boundary (i.e., for all $t \in [0, T]$) we determine a local confidence region $U_\beta(t)$ centered at the true point $s(t;\psi)$ (see Fig. 1). The size of the local confidence region depends on β, which in turn depends on the chosen local confidence level $\eta \in [0, 1]$; if $\hat{s}(t)$ is estimated using an MLE operating in the asymptotic regime, then

$$\Pr\{\hat{s}(t) \in U_\beta(t)\} = \eta.$$

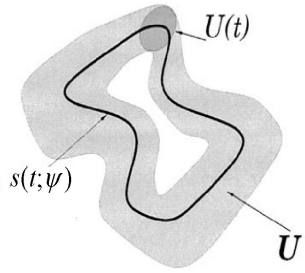

Figure 1: Local and global confidence regions (from [9]).

The details of the procedure are as follows.

1. Find the CCRLB for the shape parameters. This gives us the $P \times P$ covariance matrix $C_\psi = \mathrm{Cov}(\psi)$.

2. For all $t \in [0, T]$, compute the 2×2 matrix

$$C_s(t) = [\nabla_\psi s(t;\psi)]^T C_\psi \nabla_\psi s(t;\psi). \tag{19}$$

3. Choose a local confidence level $\eta \in [0, 1]$.

4. The local confidence region is the ellipse

$$U_\beta(t) = \{x \in \Re^2 : (x - s(t))^T C_s(t)^{-1} (x - s(t)) \leq \beta^2\}, \tag{20}$$

where β is estimated by assuming that the left-hand side of (20) is a Chi-square random variable of degree 2 such that the probability that it is less than or equal to β^2 is η.

Since each region is an ellipse, the $U_\beta(t)$'s are also referred to as local confidence ellipses. A global confidence region

$$U_\beta = \bigcup_{t \in [0,T]} U_\beta(t)$$

can now be determined by moving these ellipses along the boundary, as in Fig. 1.

We have parameterized the shape using its EGI; see Section 2. Therefore the function $s(t)$ brings us back from the EGI domain to the cartesian coordinate system by

$$s(t;\psi) = \left[\sum_{i=1}^{t} a_i \cos\left(\theta_i + \frac{\pi}{2}\right), \sum_{i=1}^{t} a_i \sin\left(\theta_i + \frac{\pi}{2}\right) \right]^T \tag{21}$$

where t takes the discrete values $t = 1, \ldots, N$. Each value of t indexes a vertex of the polygon and thus we can find the local confidence ellipses centered at all the vertices. Note that we used the CCRLB evaluated in Section 4 to form the confidence regions; the covariance matrix C_ψ in (19) is obtained from (18) and is a $2N \times 2N$ matrix for an N-sided polygon. The constraints (5) and (6) imply that when $t = N$, (21) gives $s(N;\psi) = [0,0]^T$, so that the convex polygon produced, while symmetric, actually has its Nth vertex at the origin. Since this point is technically determined, there is no uncertainty associated with it; rather there is an induced uncertainty about the centroid of the polygon. However, we chose to plot the final region with the polygon centered at the origin. Then the symmetry of the polygon implies that the local confidence ellipse for the last vertex ($t = N$), is the reflection in the origin of that for its corresponding vertex ($t = N/2$).

6 Results

Fig. 2 shows the local confidence ellipses for an origin-symmetric, regular polygon with $N = 12$ sides. The brightness function was measured from $M = 36$ equally spaced viewing angles in the range $[0, \pi]$. The noise corrupting the brightness function measurements is assumed to be $N(0, \sigma^2)$ with $\sigma = 0.05$, and the local confidence level η=0.73. Due to the parametrization in (21), if the starting vertex of the polygon is shifted, the local confidence regions also shift accordingly. We observe in Fig. 2 that the ellipses are not all the same; this is due to error propagation along the vertices (see [7]).

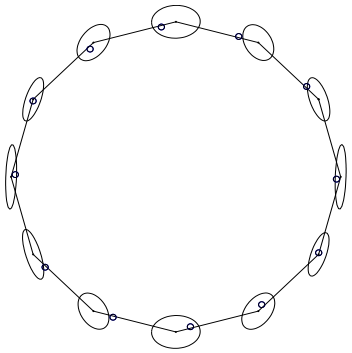

Figure 2: Local confidence regions for a polygon.

The very small circles in Fig. 2 indicate the vertices of the output polygon from our shape reconstruction algorithm (see [2], [3], and [7]) from these noisy measurements. We have found that the ellipses seen in Fig. 2 increase in size as the noise increases and also as η increases, as one would expect.

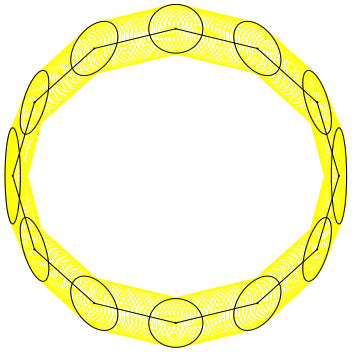

Figure 3: Confidence regions with fewer observations.

Fig. 3 shows the local confidence regions for the same polygon, but when the brightness function is measured from only $M = 18$ equally spaced viewing angles in the range $[0, \pi]$. The ellipses are larger, as expected since there is less information. There are methods to obtain the confidence region of a line segment using the confidence regions of its end points (see [7]) and we have used them in Fig. 3 to obtain a confidence region for the entire boundary.

The input polygon for Figs. 4 and 5 is an origin-symmetric, affinely regular polygon with $N = 12$ sides. The eccentricity ρ of the polygon, that of the ellipse in which it is inscribed, is $\rho = 1.54$. Again, $M = 36$, $\sigma = 0.05$, and $\eta = 0.73$. For Fig. 4, observations

were from angles equally spaced in the range $[0, \pi]$. The local confidence ellipses are larger than those in Fig. 2, indicating that its more difficult to estimate shapes with higher eccentricities. For Fig. 5, we took more observations from angles near the direction of eccentricity (elongation), thus obtaining more information near that direction. Though the total number of observations is the same, this choice of viewing directions resulted in smaller local confidence regions for the same polygon compared to those in Fig. 4.

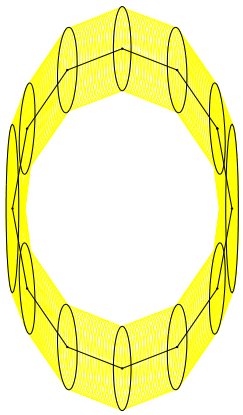

Figure 4: Confidence regions for a polygon with higher eccentricity.

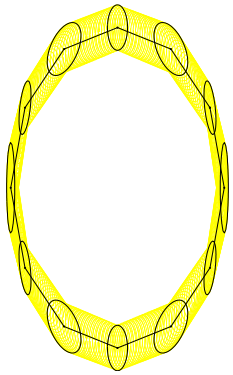

Figure 5: Confidence regions with a better set of viewing directions.

7 Conclusion

Unconstrained CRLB analysis for the problem of shape reconstruction from brightness functions confirmed the fact that the solution is not unique. Constraints for origin symmetry were incorporated in the analysis to obtain the CCRLB. Using this, the asymptotic local and global confidence regions for the estimated parametric 2-D shape boundary were obtained.

The behavior of the confidence regions is intuitive. The size of the local confidence regions gives the amount of uncertainty, which increases as the noise corrupting the brightness function measurements increases. As the number of observations increases, the uncertainty decreases. The size of the confidence regions also increases with the local confidence level. Finally, for eccentric bodies the uncertainty is much higher near the direction of eccentricity, but this can be reduced by choosing a better set of viewing directions.

References

[1] R. J. Gardner, "Geometric Tomography", Cambridge University Press, New York, 1995.

[2] R. J. Gardner and P. Milanfar, "Shape reconstruction from brightness functions", *SPIE Conference on Advanced Signal Processing Algorithms, Architectures, and Implementations X*, Vol. 4474, August 2001, San Diego, CA.

[3] R. J. Gardner and P. Milanfar, "Reconstruction of convex bodies from brightness functions", *Disc. Comput. Geom.*, to appear.

[4] B. K. P. Horn, E. J. Weldon Jr., "Filtering closed curves", *IEEE Trans. on Pattern Analysis and Machine Intelligence*, 8(5):665-678, 1986.

[5] Steven Kay, "Fundamentals of Statistical Signal Processing", Prentice-Hall, Englewood Cliffs, NJ, 1993.

[6] A. S. Lele, S. R. Kulkarni, and A. S. Willsky, "Convex polygon estimation from support line measurements and applications to target reconstruction from laser radar data", *J. Optical Soc. Amer. A*, 9:1693-1714, 1992.

[7] A. Poonawala, "Reconstructing Shape Using Brightness Functions - A Statistical Analysis", Masters Thesis, in progress.

[8] P. Stoica and B. C. Ng, "On the Cramér-Rao bound under parametric constraints", *IEEE Signal Processing Letters*, 5(7):177-179, 1998.

[9] J. C. Ye, Y. Bresler, and P. Moulin, "Asymptotic global confidence regions in parametric shape estimation problems", *IEEE Trans. on Information Theory*, 46(5):1881 -1895, 2000.